

# Large Plasma Pressure Perturbations and Radial Convective Transport in a Tokamak

KRASHENINNIKOV Sergei, RYUTOV Dmitri<sup>1</sup> and YU Guanghui

*University of California at San Diego, La Jolla, CA 92093, USA*

<sup>1</sup>*Lawrence Livermore National Laboratory, Livermore, CA 94551, USA*

(Received: 9 December 2003 / Accepted: 3 April 2004)

## Abstract

Strongly localized plasma structures with large pressure inhomogeneities (such as plasma blobs in the scrape-off-layer (SOL)/shadow regions, pellet clouds, Edge Localized Modes (ELMs)) observed in the tokamaks, stellarators and linear plasma devices. Experimental studies of these phenomena reveal striking similarities including more convective rather than diffusive radial plasma transport. We suggest that rather simple models can describe many essentials of blobs, ELMs, and pellet clouds dynamics. The main ingredient of these models is the effective plasma gravity caused by magnetic curvature, centrifugal or friction forces effects. As a result, the equations governing plasma transport in such localized structures appear to be rather similar to that used to describe nonlinear evolution of thermal convection in the Boussinesq approximation (directly related to the Rayleigh-Taylor (RT) instability).

## Keywords:

pressure perturbation, pellet cloud, ELM, blob, convective transport, Rayleigh-Taylor instability

## 1. Introduction

In many cases strongly localized, in the plane perpendicular to the magnetic field lines, plasma pressure inhomogeneities emerge in tokamaks. The examples of such cases are the plasma blobs in the SOL [1-8], pellet clouds [9,10], ELMs [11,12]. Even though at first glance they look very different, they all exhibit more convective rather than diffusive radial transport of a plasma. Similar features of convective crossfield plasma transport toward the wall were observed also in stellarators [13] and linear plasma devices [14,15].

Rather detailed experimental study of these phenomena shows striking similarities between them. For example, the temporal profiles of ion saturation currents in plasma blobs, measured by probes, in tokamak SOL [1] and in the shadows of linear devices [15] look virtually the same. Another example is the similarities in probe measurements of plasma blobs in both L- and H-modes and ELMs, although of relatively small amplitudes which do not damage the probe, [11].

In this paper we suggest that rather simple two-dimensional (2D) models can describe many essentials of blobs, small ELMs, and pellet clouds dynamics. The main ingredient of these models based on an ideal magnetohydrodynamics (MHD) is the effective plasma gravity caused by magnetic curvature, centrifugal or friction forces effects. As a result, the equations governing plasma transport in blobs, small ELMs, and pellet clouds appear to be rather similar to those used to describe nonlinear evolution of the RT instability

[16]. Therefore, it is not surprising that all these plasma physics phenomena have many similar features.

The paper is organized as follows. In Sec. 2 we review equations describing blob dynamics in the far SOL [6] and in the shadows of linear devices [17], as well as discuss the results of both analytic and numerical solution of these equations [6,18]. In Sec. 3 we derive equations describing blob dynamics in the vicinity of the separatrix to account for the effects of cross-field conductivity [19] caused by a strong shear of the magnetic field near the X-point [20]. Based on these equations we are also presenting the estimates of the blob radial velocity in the region close to separatrix. In Sec. 4 we discuss the equations, which can be used to model main features of the dynamics of blobs with large plasma beta and show their similarity to studies of evolution of pellet clouds [9,10]. We also present some results of numerical modeling of these equations. In Sec. 5 we discuss the material presented in previous Sections in the context of the studies of nonlinear evolution of RT instability and summarize our main conclusions.

## 2. Blob dynamics in far SOL of tokamak and shadow of linear device

In order to explain experimental results [21] of fast radial transport of plasma through the SOL of main chamber a simple 2D model was suggested in [6]. The main idea of this

model can be described as follows. Time to time, due to some nonlinear processes, the plasma blobs (filaments, extended along the magnetic field lines and seen on visual diagnostics [3] as a blob) are peeled off from the bulk plasma and move radially through the SOL toward the wall with high speed due to  $\nabla B$  plasma polarization and corresponding  $\mathbf{E} \times \mathbf{B}$  drift. The plasma density in the blob is much higher than ambient plasma density in far SOL and comparable to that of the bulk plasma in the vicinity of the separatrix. Therefore, even though blobs are peeled off the bulk not often, their contributions to plasma energy and particle transport in far SOL can be dominant. In linear devices the role of  $\nabla B$  in plasma polarization can be played by centrifugal force or neutral wind effects [17]. We notice that this physical picture of dominant role of blobs in plasma transport in tokamak far SOL and the shadows of linear devices was later supported by experimental observations in both tokamaks and linear devices.

To describe blob dynamics in tokamak far SOL we use quasi-slab approximation of the outer side of the torus, with  $x$  and  $y$  coordinates being radial and poloidal directions and straight magnetic field lines intersecting material surfaces situated at distance  $L_c$  (with the subscript “c” standing for “connection”) from each other (see Fig. 1). We assume cold ions and fixed electron temperature ( $T_e$ ) which is uniform and constant in time. Then in electrostatic approximation from electron and ion momentum balance equations and  $\nabla \cdot \mathbf{j} = 0$ , where  $\mathbf{j}$  is the electric current, we find

$$\nabla_{\perp} \cdot \left\{ \frac{cnT_e}{\Omega_i B} \frac{d\nabla_{\perp} \phi}{dt} \right\} + \frac{2}{R} \frac{cT_e}{B} \frac{\partial n}{\partial y} = \nabla_{\parallel} j_{\parallel}, \quad (1)$$

where  $R$  is the tokamak major radius,  $n$  is the plasma density,  $B \propto 1/R$  is the toroidal magnetic field strength,  $\Omega_i$  is the ion-cyclotron frequency,  $c$  is the light speed,  $\phi = e\varphi/T_e$ ,  $e$  is the elementary charge,  $\varphi$  is the electrostatic potential,  $d(\dots)/dt = \partial(\dots)/\partial t + \mathbf{u}_{E \times B} \cdot \nabla(\dots)$ ,  $\mathbf{u}_{E \times B} = c(\mathbf{B} \times \nabla\varphi)/B^2$ ,  $j_{\parallel}$  is the parallel current.

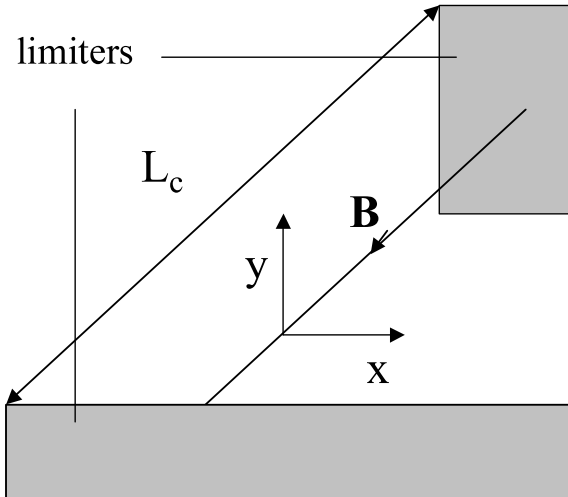


Fig. 1 Schematic view of the SOL region.

Assuming low plasma volumetric resistivity and constant plasma density along the magnetic field lines we integrate the equation (1) along parallel coordinate and find

$$\nabla_{\perp} \cdot \left\{ \frac{cnT_e}{\Omega_i B} \frac{d\nabla_{\perp} \phi}{dt} \right\} + \frac{2}{R} \frac{cT_e}{B} \frac{\partial n}{\partial y} = \frac{j_{\parallel}(1) - j_{\parallel}(2)}{L_c}, \quad (2)$$

where  $j_{\parallel}(1)$  and  $j_{\parallel}(2)$  are the currents to the walls

$$j_{\parallel}(\text{wall}) = s_w en C_s \left\{ 1 - \left( \frac{M}{2\pi m} \right)^{1/2} \exp(\phi_w - \phi) \right\}, \quad (3)$$

$M$  and  $m$  are the ion and electron masses respectively,  $C_s = (T_e/M)^{1/2}$ ,  $s_w = \pm 1$  depending on the orientation of the wall with respect to the coordinate frame,  $\phi_w$  is the potential of the wall (here we assume  $\phi_w = \text{const.}$ ). For relatively small fluctuating part of electrostatic potential,  $|\phi| < 1$ , from (3) we have  $j_{\parallel}(\text{wall}) = \sigma_w en C_s \phi$ . Substituting this expression in (2) we find

$$\rho_s^2 \nabla_{\perp} \cdot \left\{ n \frac{d\nabla_{\perp} \phi}{dt} \right\} + \frac{2\rho_s C_s}{R} \frac{\partial n}{\partial y} = \frac{2C_s}{L_c} n \phi, \quad (4)$$

where  $\rho_s = C_s/\Omega_i$ . Equation (4) with the continuity equation

$$\frac{\partial n}{\partial t} + \mathbf{u}_{E \times B} \cdot \nabla n = - \frac{2C_s}{L_c} n, \quad (5)$$

govern blob dynamics in far SOL region (the term in right hand side of eq. (5) describes plasma leakage to material surface along the magnetic field lines).

In the absence of ambient plasma the eqs. (4) and (5) allow the solution in the form of traveling wave (blob) [6],

$$n(x, y, t) = n_b(x - V_b t) \exp \left\{ - \left( \frac{y}{\delta_y} \right)^2 - \frac{2C_s t}{L_c} \right\}, \quad (6)$$

where  $n_b(x)$  is an arbitrary function,  $\delta_y$  is the effective poloidal width of the blob, and

$$V_b = 2C_s \left( \frac{\rho_s}{\delta_y} \right)^2 \frac{L_c}{R} \quad (7)$$

is the velocity of the blob. For  $T_e \sim 30\text{eV}$ ,  $B \sim 2\text{T}$ ,  $\delta_y \sim 1\text{cm}$ ,  $L_c \sim qR$ , where  $q$  is the safety factor ( $\sim 3$ ), from eq. (7) we find  $V_b \sim 10^5 \text{ cm/s}$ , which is close to the experimental observations [1-5].

In the case of linear devices, where there are no magnetic field curvature effects, plasma polarization can be due to centrifugal force or neutral wind. The later one is related to asymmetry in neutrals distribution function [17]. The neutrals coming to the wall from plasma side experienced some plasma-neutral interactions. Therefore, they are hotter than the neutrals coming from the wall. As a result of this asymmetry, in the shadow regions of linear devices there is neutral-ion friction force (neutral wind) even though neutral particle flux is negligibly small. In a sense, neutral wind is an extension of thermal force to the semi-collisional situation.

Taking neutral wind effects into account, the analog of eq. (4) can be written as follows

$$\rho_s^2 \nabla_{\perp} \cdot \left\{ n \frac{d \nabla_{\perp} \phi}{dt} \right\} + C_s \eta_{polar} \frac{\partial n}{\partial y} = \frac{2C_s}{L_c} n \phi, \quad (8)$$

where  $\eta_{polar} \sim v_{iN}/\Omega_i$  is the plasma polarization factor and  $v_{iN}$  is the ion-neutral collision frequency. Notice that with replacement  $\eta_{polar} \sim v_{iN}/\Omega_i$  on  $\eta_{polar} = 2\rho_s/R$  the eqs. (4) and (8) are virtually the same. It explains the similarities of blobs in tokamak SOL and shadows in linear devices seen in experiments.

Study of blob dynamics governed by eqs. (8) and (5) shows [18] that the blobs with crossfield scale

$$\delta_b \sim \delta_* = 2\rho_s \left( \frac{L_e}{\rho_s} \right)^{2/5} (\eta_{polar})^{1/5} \quad (9)$$

(we assume here that  $\delta_b \equiv \delta_y \sim \delta_x$ ) are very stable structurally and propagate radially on large distance keeping its shape intact. Blobs bigger than  $\delta_*$  are the subjects of the RT instability, which splits them in a few smaller ones. Blobs smaller than  $\delta_*$  are quickly transformed into mushroom shape with thin front like structures [8] and their further evolution is sensitive even to weak plasma diffusion.

### 3. Blob dynamics in the vicinity of separatrix

In previous section we analyzed blob dynamics in tokamak far SOL where magnetic field lines have a very simple geometry. However, blobs are peeled off from bulk plasma in the vicinity of the separatrix (in diverted tokamaks). To describe blob dynamics there we need to account for geometrical effects of a strong shear of the magnetic field near the X-point. In [20] it was shown that magnetic shear in the vicinity of X-point results in dramatic squeezing of magnetic flux tubes. Figure 2 shows this schematically. The shadowed regions represent the same flux tube when it passes near the X-point, from the position 1 in the main SOL, to position 3 in

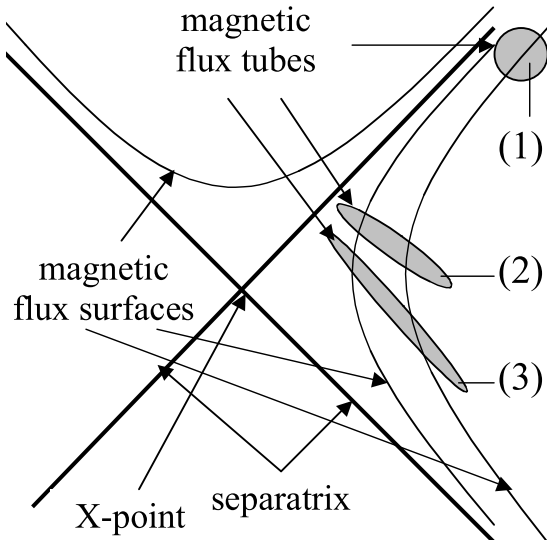


Fig. 2 Evolution of the cross-section of magnetic flux tube in the vicinity of separatrix

the divertor leg. Due to a very strong squeezing of the tube in the vicinity of X-point, its minimal width for standard tokamak conditions decreases from  $\sim 1$  cm around the mid-plane to less than the ion gyro-radius close to X-point [20]. As a result, the effects of finite cross-field resistivity, otherwise small, are strongly magnified [19,22] and play an important role.

In order to incorporate these effects into our simplified physical picture of blob dynamics we will use a heuristic model developed in [19]. The essence of this model is the substitution of exact solution of penetration of the electrostatic potential into X-point region by an effective boundary condition relating parallel current and potential at the entrance to the X-point region. To derive this relation, we take into account squeezing of the flux tube we introduce: a) squeezing function  $S(\ell) \approx \exp(-\ell/L_X)$ , where  $\ell$  is the length along the magnetic field line and  $L_X$  is the effective squeezing length (usually in current large tokamaks  $L_X \sim 10^3$  cm), and b) the effective wave number of the potential perturbation  $K(\ell) = k/S(\ell)$ , where  $k$  is the wave number at the entrance into the X-point region. Then, we balance perpendicular,  $j_{\perp} = -i\sigma_{\perp}K(\ell)\phi$ , and parallel,  $j_{\parallel} = -\sigma_{\parallel}(\partial\phi/\partial\ell)$ , currents via the  $\nabla \cdot j = 0$  equation,  $\partial^2\phi/\partial\ell^2 = -(\sigma_{\perp}/\sigma_{\parallel})K^2(\ell)\phi$ , where  $\sigma_{\perp} = \omega_{pe}^2/v_e/(4\pi\Omega_e^2)$  and  $\sigma_{\parallel} = \omega_{pe}^2/(4\pi v_{ei})$  (notation is standard). As a result, we find a relation between parallel current and electrostatic potential at the entrance to the X-point region [19]

$$j_{\parallel}|_{entr} \approx \sigma_{eff} |k|\phi|_{entr}, \quad (10)$$

where  $\sigma_{eff} = G\omega_{pe}^2/(4\pi\Omega_e)$ , and  $G$  is order unity phenomenological coefficient. Notice that the squeezing of the magnetic flux tube occurs near the separatrix in both open and closed flux surfaces and, therefore, the expression (10) can be applied at both sides from the separatrix.

We can use the relation (10) to close eq. (1) after the integration along the magnetic field like as we did in Sec. 2, where magnetic field lines were going through the wall and we used relation (3) to close eq. (2). For simplicity, we consider only a symmetric double-null divertor, so that eq. (10) should be applied at both ends of the flux tube (with the obvious change of the sign). Then, approximating wave number of the blob at the entrance into the X-point region as  $k \sim 1/\delta_b$  we find

$$\rho_s^2 \nabla_{\perp} \cdot \left\{ n \frac{d \nabla_{\perp} \phi}{dt} \right\} + \frac{2\rho_s C_s}{R} \frac{\partial n}{\partial y} = \frac{2C_s}{L_b} \frac{\rho_s}{\delta_b} G n \phi, \quad (11)$$

where  $L_b$  is the parallel length of the blob. From eq. (11) we estimate radial velocity of the blob

$$V_b \sim \frac{2C_s}{G} \frac{\rho_s}{\delta_b} \frac{L_b}{R}. \quad (12)$$

Thus we find that strong squeezing of magnetic flux tube in the vicinity of X-point do not prohibit the blob radial motion. By taking into account effective X-point resistivity [19] we describe blob motion in the vicinity of the separatrix in both closed and open magnetic flux surfaces. Moreover, compar-

ing the expressions (7) and (12) we see that close to the separatrix  $V_b \propto \rho_s/\delta_b \ll 1$ , while in the far SOL  $V_b \propto (\rho_s/\delta_b)^2$ . Therefore, it can explain experimental observations [5] of higher blob velocity in the region close to the separatrix than in far SOL.

#### 4. Dynamics of blobs with large beta

In previous sections we neglected an impact of blob on the structure of the magnetic field. However, in case of large beta of blob plasma,  $\beta_b$ , such impact can be very important. In order to address this issue we estimate the perturbation of the magnetic field due to the blob motion in a tokamak. In this case, the plasma polarization current is balanced by parallel current dipole

$$j_{\parallel} \sim enC_s \frac{\rho_s}{\delta_b} \frac{L_b}{R}, \quad (13)$$

which gives the following magnitude of radial perturbation of the magnetic field strength,  $B_r$ ,

$$\frac{B_r}{B} \sim \frac{4\pi}{c} j_{\parallel} \delta_b \sim \beta_b \frac{L_b}{R}. \quad (14)$$

As a result, the magnetic field line bends in radial direction. Since bending of magnetic field like propagates along  $\mathbf{B}$  with the Alfvén velocity  $V_A = B/(4\pi nM)^{1/2}$  such quasi-steady state approximation of the magnetic field line structure can be considered if

$$\frac{V_b}{V_A} \gtrsim \frac{B_r}{B} \sim \beta_b \frac{L_b}{R}. \quad (15)$$

Then, taking into account the expressions (7) and (12) for blob velocity, we find from inequality (15):

$$V_b < C_s \beta_b^{1/2} \frac{L_b}{R}. \quad (16)$$

However, at relatively large  $\beta_b$  bending of the magnetic field lines becomes so strong that the magnetic field line would “touch” first wall without even going through the material surfaces of divertor targets or limiters (see Fig. 3). Taking into account expression (14) from Fig. 3 one sees that such situation occurs for

$$\beta_b > \beta_{crit} \sim \frac{R\Delta_w}{L_c^2}, \quad (17)$$

where we assume  $L_b \approx L_c$ ,  $\Delta_w$  is the distance from last closed flux surface to the first wall. In order to describe the evolution of blobs with  $\beta_b > \beta_{crit}$  within the framework of simple 2D model, we use the approach adopted in the studies of the dynamics of pellet clouds [9,10]. Introducing the vector potential  $A_{\parallel}$  and taking into account that the bending of magnetic field propagates along the field line with Alfvén speed, from relation  $E_{\parallel} = -\nabla_{\parallel}\phi - c^{-1}\partial A_{\parallel}/\partial t = 0$  we find  $\phi = (V_A/c)A_{\parallel}$  and, correspondingly,

$$j_{\parallel} = -\frac{c^2}{4\pi V_A} \nabla_{\perp}^2 \phi. \quad (18)$$

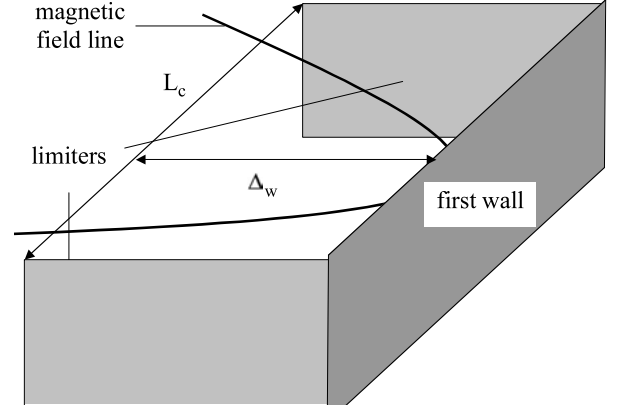


Fig. 3 Strong bending of magnetic field line causes touch of first wall without intersection of limiters.

Substituting (18) in (2) we have

$$\rho_s \nabla_{\perp} \cdot \left\{ n \frac{d\nabla_{\perp} \phi}{dt} \right\} + \frac{2C_s}{R} \frac{\partial n}{\partial y} = -\frac{2V_A}{L_b} n_{amb} \rho_s \nabla_{\perp}^2 \phi, \quad (19)$$

where the Alfvén velocity is calculated with the density of ambient plasma  $n_{amb} = \text{const}$ . The eq. (19) is just the same as the equation describing the evolution of pellet clouds in [9, 10]. From eq. (19) it is possible to show that for large blobs, where inertial term in (19) is small, the velocity of the blob described by eq. (19) does not depend of its spatial scale and can be estimated as follows

$$V_b \sim C_s \frac{C_s}{V_A} \frac{L_b}{R} = C_s \sqrt{\beta} \frac{L_b}{R}. \quad (20)$$

The results of numerical solution of eq. (19) support estimate (20). In Fig. 4 we show how seeded blob, described by eq. (19), coherently moves in the radial direction ( $R = 175$  cm,  $L_b = 4000$  cm,  $\rho_s = 0.06$  cm,  $V_A = 4 \times 10^9$  cm/s,  $C_s = 3 \times 10^6$  cm/s).

#### 5. Discussions

Thus we find that the blob dynamics in edge plasmas can be described with rather similar eqs. (8), (11) and (19), depending on plasma conditions and geometry. In some sense these equations are similar to the Boussinesq approximation of 2D thermal convection (related to the Rayleigh-Taylor instability of a stratified medium)

$$d_t \nabla_{\perp}^2 \psi + g \frac{\partial T}{\partial y} = \mu \nabla_{\perp}^4 \psi, \quad d_t T = 0, \quad (21)$$

where  $T$  is the temperature,  $g$  is the effective gravity acceleration,  $\mathbf{u} = \mathbf{e}_z \times \nabla \psi$  is the velocity,  $\mu$  is the effective viscosity. However, “dissipative” terms in right hand side of the blob equations are different than in (21). In case where dissipation is not important we see that mushroom shape of originally circular blob develops (see for example [8,18]) similar to the typical mushrooms shapes in the dynamics of the RT instability [16]. But, “dissipative” terms can bring structural stability of blobs when they propagate on large distance as a

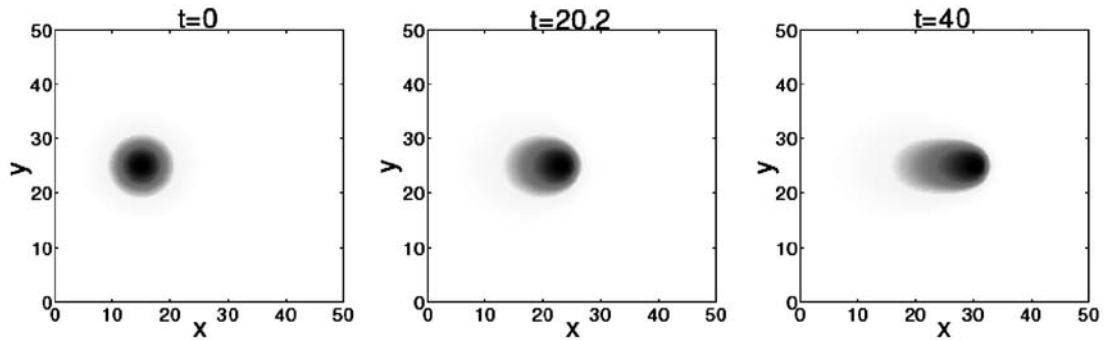


Fig. 4 Density contours of blob.

coherent structure [6,8,18].

We also find that the dynamics of blobs with high beta can be described by the same equations as the evolution of pellet clouds [9,10]. As a matter of fact, this is not surprising since in both cases we consider the evolution of plasma structures with the pressure, which significantly exceeds the pressure of a surrounding tokamak plasma. Therefore, this may be a reasonable model for the studies of nonlinear dynamics of large pressure perturbations of relatively small spatial scale when perturbations can be treated like isolated filaments.

One of the examples of such process can be ELM of small amplitude, when tokamak edge plasma is not perturbed too much, and isolated features of ELM structure are clearly seen in the experiment [5,11]. According to our findings described above, small isolated ELM propagates in convective manner through the edge and SOL plasmas somewhat similar to what was observed in experiment [5,11]. This is different from the results of [23] where early nonlinear stage of ballooning instabilities was considered and explosive type of behavior was predicted. It is plausible that early nonlinear evolution goes with some acceleration and then, in a deeply nonlinear stage, evolution converges into nonlinear advection of pressure perturbation which is characterized by more or less constant speed. Clearly additional studies are needed to clean this issue up.

The work was performed for the U.S. DoE under contract W-7405-Eng-48 at the LLNL and Grant No. DE-FG03-00ER54568 at the UCSD.

### References

- [1] J.A. Boedo, D.L. Rudakov, R.A. Moyer *et al.*, Phys. Plasmas **8**, 4826 (2001).
- [2] J.J.L. Terry, R. Maqueda, C.S. Pitcher *et al.*, J. Nucl. Mater. **290-293**, 757 (2001).
- [3] S.J. Zweben, D.P. Stotler, J.L. Terry *et al.*, Phys. Plasmas **9**, 1981 (2002).
- [4] G.Y. Antar, G. Counsell, Y. Yu *et al.*, Phys. Plasmas **10**, 419 (2003).
- [5] J.A. Boedo, D.L. Rudakov, R.A. Moyer *et al.*, Phys. Plasmas **10**, 1670 (2003).
- [6] S.I. Krasheninnikov, Phys. Lett. A **283**, 368 (2001).
- [7] D.A. D'Ippolito, J.R. Myra, and S.I. Krasheninnikov, Phys. Plasmas **9**, 222 (2002).
- [8] N. Bian, S. Benkadda, J.-V. Paulsen *et al.*, Phys. Plasmas **10**, 671 (2003).
- [9] V. Rozhansky, I. Veselova and S. Voskoboynikov, Plasma Phys. Control. Fusion **37**, 399 (1995).
- [10] P.B. Parks, W.D. Sessions and L.R. Baylor, Phys. Plasmas **7**, 1968 (2000).
- [11] D.L. Rudakov, J.I. Boedo, R.A. Moyer *et al.*, Plasma Phys. Control. Fusion **44**, 717 (2002).
- [12] G. Counsell *et al.*, *19<sup>th</sup> IAEA Fusion Energy Conf., Lyon, France, 14-19 Oct., 2002*, Paper IAEA-CN-94/EX/D1-2.
- [13] E. Sanchez, C. Hidalgo, C. Riccardi *et al.*, Phys. Plasmas **7**, 1408 (2000).
- [14] G.Y. Antar, S.I. Krasheninnikov, P. Devynck *et al.*, Phys. Rev. Lett. **87**, 065001 (2001).
- [15] T. Carter, Bull. Am. Phys. Soc. **47**, 201 (2002).
- [16] Y.-N. Young, H. Tufo, A. Dubey and R. Rosner, J. Fluid Mech. **447** 377 (2001).
- [17] S.I. Krasheninnikov and A.I. Smolyakov, Phys. Plasmas **10**, 3020 (2003).
- [18] G.Q. Yu and S.I. Krasheninnikov, Phys. Plasmas **10**, 4413 (2003).
- [19] D.D. Ryutov and R.H. Cohen, *to appear in Contributions to Plasma Physics* (2004).
- [20] D. Farina, R. Pozzoli and D.D. Ryutov, Nucl. Fusion **33**, 1315 (1993).
- [21] M.V. Umansky, S.I. Krasheninnikov, B. LaBombard and J.L. Terry, Phys. Plasmas **5**, 3373 (1998).
- [22] J.R. Myra, D.A. D'Ippolito, X.Q. Xu and R.H. Cohen, Phys. Plasmas **7**, 2290 (2000).
- [23] S.C. Cowley, H. Wilson, O. Hurricane and B. Fong, Plasma Phys. Control. Fusion **45**, A31 (2003).